ELSEVIER

Chemical Engineering Science 60 (2005) 1155–1166

Chemical Engineering Science

www.elsevier.com/locate/ces

On the Langmuir–Hinshelwood formulation for zeolite catalysed reactions

R. Krishna*, R. Baur

Van 't Hoff Institute for Molecular Sciences, University of Amsterdam, Nieuwe Achtergracht 166, 1018 WV Amsterdam, The Netherlands

Received 10 May 2004; received in revised form 28 August 2004; accepted 23 September 2004

Abstract

The Langmuir–Hinshelwood (LH) rate expression is often used to describe the kinetics of heterogeneously catalysed reactions using zeolites. A factor $\theta_V^n \equiv (1-\sum_i \theta_i)^n$ in the LH expression allows for the reduction of the reaction rate with increased fractional occupancies θ_i of the individual species involved in an n-molecular reaction on the catalyst surface. Most commonly in practice the multicomponent Langmuir (MCL) approach is used for calculation of the fractional occupancies giving $\theta_V \equiv 1/(1+\sum_i b_i p_i)$ where the b_i are the Langmuir adsorption constants and p_i are the partial pressures in the gas phase. The LH-MCL approach is, however, thermodynamically consistent only when the saturation capacities of all the individual species in the mixture are identical to one another, or when the component loadings are small. For mixtures containing molecules with different saturation capacities, the sorption loadings are significantly affected by entropy effects, especially for high loadings within the zeolite catalyst. In the general case we need to determine the sorption loadings, and occupancies, using the Ideal Adsorbed Solution Theory. Using the gas phase isomerization of n-hexane with MFI zeolite catalyst as an illustration we demonstrate the limitations of the LH-MCL kinetics for calculation of reactor conversions. More significantly, we demonstrate how entropy effects can be exploited in simulated moving bed reactor configuration to obtain supra-equilibrium conversions and improved reaction selectivities.

Keywords: Zeolite catalysis; Isomerization; Molecular simulations; Packed bed reactor; Simulated moving bed reactor; Langmuir–Hinshelwood kinetics; Ideal adsorbed solution theory; Entropy effects; MFI zeolite

1. Introduction

Zeolites are widely used in the processing industries to catalyse a variety of reactions such as cracking, oxidation, isomerization, and alkylation (Corma, 2003; Degnan and Thomas, 2003; Marcilly, 2003). The reaction kinetics is usually described by the Langmuir–Hinshelwood (LH) formulation (Aris, 1975). Consider the reversible isomerization reaction $A_1 \rightleftarrows A_2$ taking place in a zeolite catalyst. If the forward and backward reactions are both considered to be first order in the partial pressures p_i in the gas phase, the LH reaction rate expression is

$$r = \left(k_f p_1 - k_b p_2\right)\theta_V = \left(k_f p_1 - k_b p_2\right)\left(1-\theta_1-\theta_2\right), \qquad (1)$$

where the subscripts 1 and 2 refer to A_1 and A_2. The reaction rate is proportional to the fractional *vacancy*, θ_V on the catalyst surface. The reaction rate decreases with increasing loading on the catalyst surface. The forward and backward reaction rate constants k_f and k_b have the units $\mathrm{Pa}^{-1}\ \mathrm{s}^{-1}$. Often in practice the multi-component Langmuir (MCL) model is used to calculate the component loadings and fractional occupancies θ_i:

$$\theta_i \equiv \frac{\Theta_i}{\Theta_{i,\mathrm{sat}}} = \frac{b_i p_i}{1+b_1 p_1 + b_2 p_2}; i = 1, 2;$$

$$\theta_V = 1-\theta_1-\theta_2 = \frac{1}{1+b_1 p_1 + b_2 p_2}, \qquad (2)$$

where Θ_i are the molecular loadings, $\Theta_{i,\mathrm{sat}}$ are the saturation capacities and the b_i are the Langmuir adsorption constants. Combining Eqs. (1) and (2) yields the familiar form of the LH-MCL reaction rate expression most commonly used

* Corresponding author. Tel.: +31 20 5257007; fax: +31 20 5255604.
E-mail address: R.Krishna@uva.nl (R. Krishna).

0009-2509/$ - see front matter © 2004 Elsevier Ltd. All rights reserved.
doi:10.1016/j.ces.2004.09.077

in practice

$$r = \frac{k_f p_1 - k_b p_2}{1 + b_1 p_1 + b_2 p_2}. \quad (3)$$

For a bi-molecular reaction $A_1 + A_2 \rightleftarrows A_3$, the corresponding LH expression is $r = \left(k_f p_1 p_2 - k_b p_3\right) \theta_V^2$ with $\theta_V = 1/\left(1 + b_1 p_1 + b_2 p_2 + b_3 p_3\right)$. Experimentalists often obtain the parameters k_f, k_b, b_1 and b_2 by *fitting* the kinetic measurements for a wide range of partial pressures p_i.

There is an important limitation of the LH-MCL expression (3) that is insufficiently recognized in the literature. This limitation arises from the fact that the calculation of the occupancies using Eq. (2) is valid only when the saturation capacities $q_{i,\text{sat}}$ are equal for all species; this point has been emphasized by Sircar (Rao and Sircar, 1999; Sircar, 1995; Sircar and Rao, 1999). When the saturation capacities of the constituent species are significantly different, subtle *entropy* effects come into play in determining mixture loadings in zeolites (Kapteijn et al., 2000; Krishna et al., 2002a,b).

The first major objective of the present communication is to highlight the importance of entropy effects on reaction rates and selectivities in zeolites. We stress the limitations of the LH-MCL approach and put forward a case for a more rigorous approach to the modelling of reaction kinetics, using the Ideal Adsorbed Solution Theory (IAST) for the estimation of component occupancies and vacancy. The second major objective is to show that a more rigorous LH-IAST approach to reaction rates will unravel novel methods to improve conversions and selectivities for equilibrium limited reversible reactions, catalysed by zeolites.

Though the specific illustrations and examples in this paper are restricted to zeolite catalysts in contact with gaseous reactants and products, many of the concepts and ideas have a more generic character.

2. Entropy effects during sorption in zeolites

Let us consider sorption of hexane isomers, *n*-hexane (*n*C6), 3-methylpentane (3MP) and 2,2 dimethylbutane (22DMB) in MFI zeolite, that consists of a set of straight channels (0.53–0.56 nm wide), intersecting with zig-zag channels (0.51–0.55 nm wide). configurational-bias Monte Carlo (CBMC) simulations of the pure component sorption isotherms of hexane isomers (Calero et al., 2001; Schenk et al., 2001b) in MFI at 362 K are shown in Fig. 1. The accuracy of the CBMC calculation techniques have been verified in several publications (Calero et al., 2001; Dubbeldam et al., 2004; Schenk et al., 2001b; Vlugt et al., 1999) in which comparisons are made with experimental data. The linear *n*C6 molecule has a chain length that is commensurate with the length of the zig-zag channels (see Fig. 2a) and a maximum of 8 molecules per unit cell can be accommodated. The configuration of di-branched 22DMB is such that these bulky, yet compact, molecules can be located only at the intersections between the straight and zig-zag channels (see Fig. 2b) and the saturation loading is restricted to 4 molecules per unit cell; see Fig. 1. The mono-branched 3MP also prefers to locate at the intersections and only at pressures exceeding 10 kPa can these molecules be pushed into the channel interiors. The saturation capacity of 3MP is 6.3 molecules per unit cell, intermediate in value between that of *n*C6 and 22DMB. The sorption hierarchy of the pure components in MFI is *n*C6 > 3MP > 22DMB.

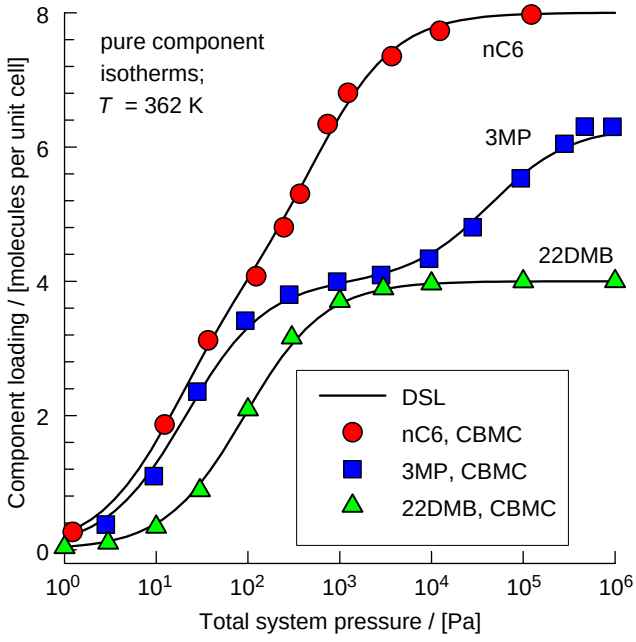

Fig. 1. Pure component sorption isotherms for *n*C6, 3MP and 22DMB in MFI at 362 K. The symbols represent CBMC simulation data (Calero et al., 2001; Krishna et al., 2002b, Schenk et al., 2001b). The continuous lines are the DSL fits using the parameters as specified in Table 1.

We also note from Fig. 1 that the dual-site Langmuir (DSL) isotherm (parameters specified in Table 1):

$$\Theta_i^0(p) \equiv \Theta_{i,A} + \Theta_{i,B} = \frac{\Theta_{i,\text{sat},A} b_{i,A} p}{1 + b_{i,A} p} + \frac{\Theta_{i,\text{sat},B} b_{i,B} p}{1 + b_{i,B} p} \quad (4)$$

provides a good description of the pure component isotherms for all three hexane isomers.

Differences in the saturation capacities of the hexane isomers have a dramatic influence on the component loadings in *mixtures*. Consider sorption of a 50–50 binary mixture of *n*C6 and 3MP in MFI. The CBMC simulations for this binary mixture are denoted by the symbols in Fig. 3a. It is interesting to note the maximum in the loading of 3MP when the total mixture loading is precisely 4 molecules per unit cell, when the intersections are all occupied; this occurs at a total pressure of about 200 Pa. When the pressure is raised above 200 Pa the loading of 3MP reduces virtually to zero. The *n*C6 has a higher packing efficiency within the MFI

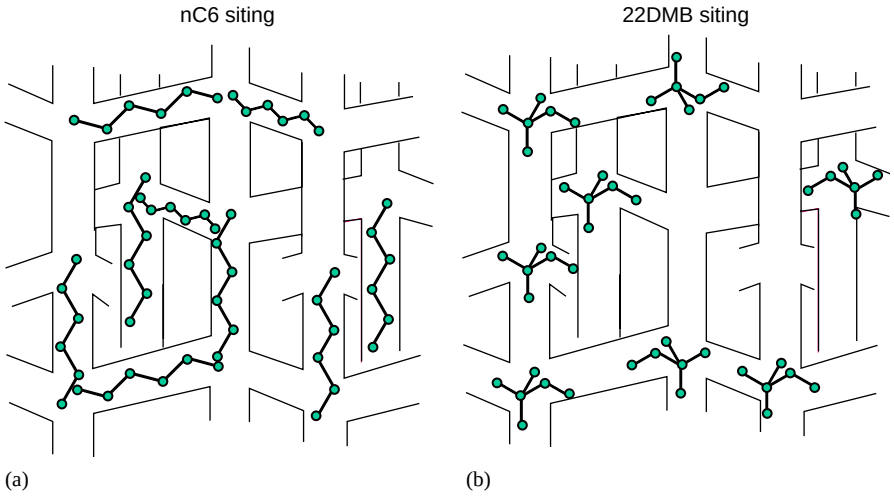

Fig. 2. (a) Schematic showing siting of *n*C6 molecules within the MFI network. (b) Schematic showing preferential location of 22DMB at intersections between straight and zig-zag channels of MFI network.

Table 1
DSL parameters for hexane isomers in MFI at 362 K

Component	Temperature [K]	DSL parameters			
		Site A		Site B	
		$b_{i,A}$ [Pa^{-1}]	$\Theta_{i,sat,A}$ [molecules per unit cell]	$b_{i,B}$ [Pa^{-1}]	$\Theta_{i,sat,B}$ [molecules per unit cell]
*n*C6	362	6.32×10^{-2}	4.0	1.7×10^{-3}	4.0
3MP	362	4.75×10^{-2}	4.0	2.27×10^{-5}	2.3
2DMB	362	1.085×10^{-2}	4.0	—	—

The fits correspond to CBMC simulations (Calero et al., 2001; Krishna and Baur, 2003b, Schenk et al., 2001b).

matrix than the 3MP molecules. It is more efficient to obtain higher loading by "replacing" the 3MP with *n*C6; this *configurational entropy* effect is the reason behind the curious maxima in the 3MP loading in then binary mixture.

An analogous behaviour is observed for sorption of a 50–50 mixture of *n*C6 and 22DMB; see Fig. 3b. At a total pressure of 200 Pa, corresponding to a total mixture loading of 4 molecules per unit cell, 22DMB exhibits a maximum in the mixture loading. When the pressure is raised above 200 Pa, the 22DMB loading is reduced to virtually zero because the di-branched isomer loses the entropic battle with the linear isomer that has a higher packing efficiency. For a 50–50 mixture of 3MP and 22DMB the entropic battle is won by the mono-branched isomer and the di-branched molecule exhibits a curious table-mountain maximum in the loading; see Fig. 3c. For an equimolar ternary mixture of *n*C6, 3MP and 22DMB both the branched isomers lose out to the linear isomer when the total system pressure exceeds about 500 Pa, at which pressure all the intersection sites are occupied. There is considerable amount of experimental evidence to support the accuracy of the CBMC simulations for estimating pure component and mixture loadings (Calero et al., 2001; Dubbeldam et al., 2004; Schenk et al., 2001b; Vlugt et al., 1999). These data also verify entropy effects described here.

Calculations on the component loadings using the MCL Eq. (2) are shown with dashed lines in Figs. 3a–d. Note that in these MCL calculations the saturation loadings of all three components are chosen to be 8 molecules per unit cell. Furthermore, the pure component isotherms have to be shoe-horned into a single-site Langmuir model, that is incapable of reflecting the inflection behaviour of 3MP. The MCL model, commonly used in the literature, is unable to account for the entropy effects prevalent at high mixture loadings and the sorption selectivity is *independent* of total system pressure and mixture loading. The IAST, developed by Myers and Prausnitz (1965) provides a reasonably good description of the mixture isotherms in zeolites (Krishna et al., 2002a). The component loadings calculated from IAST are shown by the continuous solid lines in Figs. 3a–d. The agreement with the CBMC simulations is found to be reasonably good for the whole range of pressures, also for other alkane mixtures. (Krishna and Baur, 2003b; Krishna

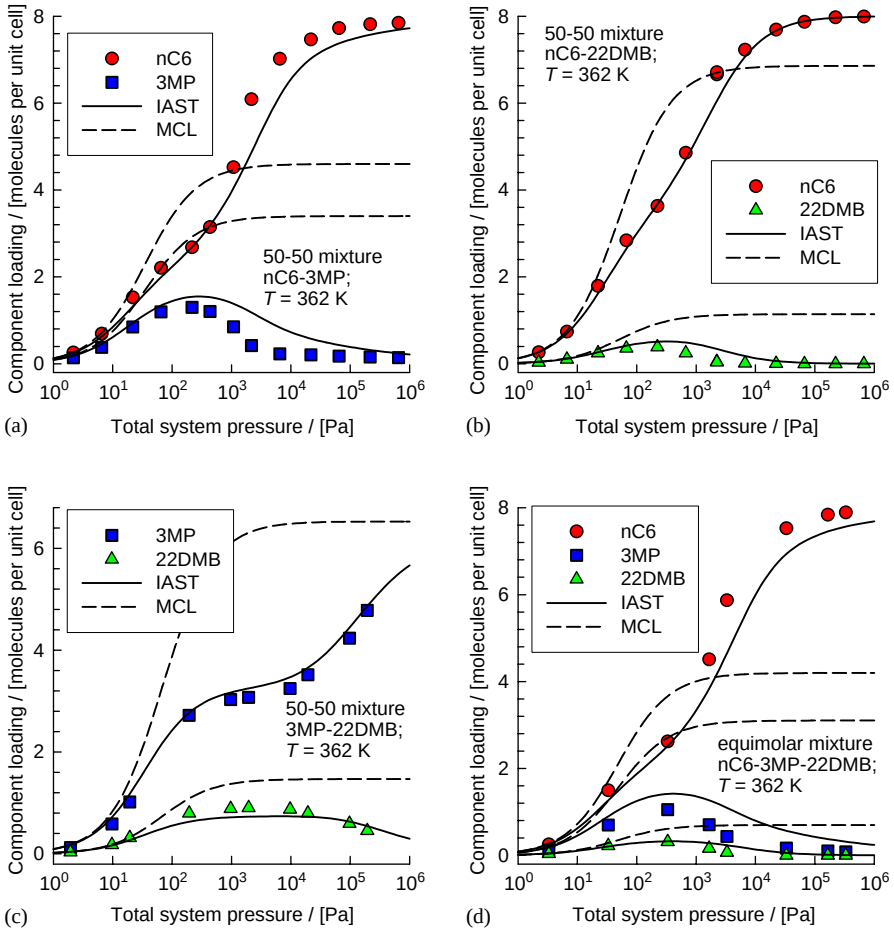

Fig. 3. CBMC simulations (denoted by symbols), of loadings in MFI zeolite at 362 K for (a) 50–50 *n*C6–3MP mixture, (b) 50–50 *n*C6–22DMB mixture, (c) 50–50 3MP–22DMB mixture, and (d) equimolar ternary *n*C6–3MP–22DMB mixture. The continuous solid lines are calculations using IAST, with the DSL parameter inputs as specified in Table 1. Calculation of the component loadings using the MCL model are shown by the dashed lines. In the MCL calculations the saturation loadings are all taken to be 8 molecules per unit cell and the Langmuir constants are 0.032445, 0.023984, 0.0054 Pa^{-1} for *n*C6, 3MP, and 22DMB, respectively.

et al., 2002a, Schenk et al., 2001b). Procedures other than the IAST for estimating the mixture loadings are found to be unsuccessful in anticipating entropy effects (Kapteijn et al., 2000; Vlugt et al., 1999).

For the equimolar ternary mixture of *n*C6, 3MP and 22DMB the calculation of the fractional vacancy θ_V using the IAST and MCL approaches are compared in Fig. 4. The IAST calculations are in good agreement with the calculations from CBMC simulations for the whole range of pressures, whereas the MCL approach predicts significantly lower vacancies with increased pressures. From the point of view of reaction rates we should expect the MCL model to significantly underestimate the reaction rate at high pressures, when compared to predictions of the IAST model.

Another type of entropy effect that can arise in zeolites relates to the relative *sizes* of the molecules. Consider, for example the adsorption of *n*-heptane (*n*C7) and *n*-nonane (*n*C9) on NaY zeolite at 503 K. The pure component isotherms, calculated using CBMC simulations (Calero et al., 2004; Denayer et al., 2003) are shown in Fig. 5a. These isotherms are best described by the DSL model with parameters specified in Table 2 The small heptane molecule has a higher saturation capacity ($q_{1,\mathrm{sat},A} = q_{1,\mathrm{sat},A} + q_{1,\mathrm{sat},B} = 1.82\,\mathrm{mol\,kg^{-1}}$) than the larger nonane molecule ($q_{2,\mathrm{sat},A} = q_{2,\mathrm{sat},A} + q_{2,\mathrm{sat},B} = 1.48\,\mathrm{mol\,kg^{-1}}$). In a 50–50 mixture of *n*C7 and *n*C9, the difference in the saturation capacities, has a profound effect on the component loadings as evidenced by CBMC simulations shown in Fig. 5b. Below a total pressure of 100 kPa, the component loading of *n*C7 is much lower than that of *n*C9. With increasing pressures the loading of *n*C7 increases at the expense of *n*C9; this is because it is easier for the smaller heptane molecule to find "gaps" in the zeolite than it is for the larger nonane molecule. This is a *size entropy* effect (Krishna et al., 2002b); this effect is so strong that it leads to a reversal of selectivity in favour of *n*C7 at saturation loadings. Denayer et al. (2003) have stressed the consequences of this selectivity reversal during hydrocracking of a 50–50 mixture of

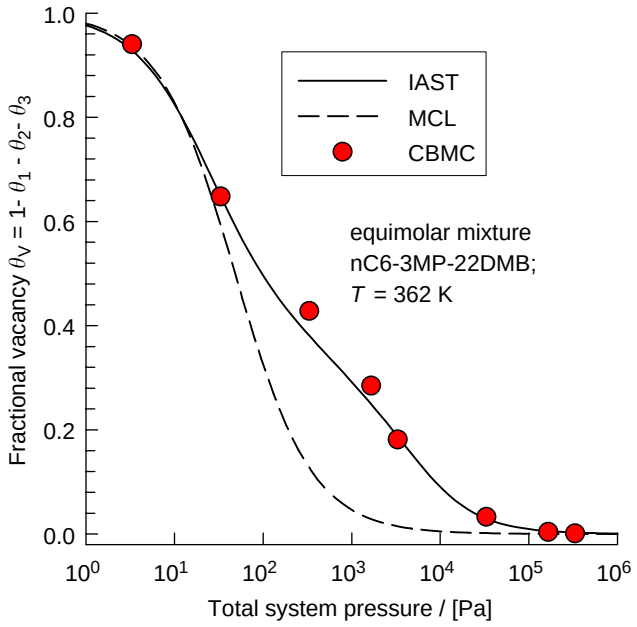

Fig. 4. Fractional vacancy for equimolar ternary mixture of C6, 3MP and 22DMB as a function of the total pressure. The continuous solid line represents calculations of θ_V using IAST, with the DSL parameter inputs as specified in Table 1. Calculation of θ_V the MCL model (2) is shown by the dashed line.

nC7 and nC9 in Pt/H-Y zeolite. At low pressure, with gas phase hydrocracking the conversion levels of nC9 are much higher than that of nC7, due to the higher concentrations of the adsorbed nC9 within the zeolite. With increasing pressures, the conversion of nC9 decreases, while that of nC7 increases and for hydrocracking in the liquid phase the nC7 conversion exceeds that of nC9. Using the MCL model (2) no selectivity reversal is predicted and furthermore, this model does not anticipate any influence of total pressure on the relative conversion of nC7 and$n$C9.

Consider the sorption of hexane isomers nC6, 3MP and 22DMB in AFI, that consists of cylindrical channels of 0.73 nm diameter. The channel dimension is large enough to accommodate the bulky 22DMB and there is therefore no configurational penalty for these molecules. However, the length of the molecules decreases with increased degree of branching (see the schematic in Fig. 6.); this implies that number of molecules that can be accommodated into the channels increases with the degree of branching. The increased sorption strength with increased branching is an entropy effect (Schenk et al., 2001a), arising because of differences in packing efficiencies within the cylindrical channels of AFI. CBMC simulations (Calero et al., 2001; Krishna et al., 2002b, Schenk et al., 2001b) of the sorption isotherms are shown in Fig. 7a. The sorption hierarchy for pressures higher than 1 kPa is found to be 22DMB > 3MP > nC6. In an equimolar ternary mixture of nC6, 3MP and 22DMB we note that entropy effects cause the linear isomer nC6, with the lowest packing efficiency, to be virtually excluded from the zeolite at high loadings; see Fig. 7b. The continuous solid lines in Fig. 7b are the predictions of the IAST using the DSL parameters specified in Table 2. We note that the IAST is able to predict the entropy effects exceedingly well and in a quantitative way.

Having stressed the importance of entropy effects during sorption in zeolites, we now focus on the influence of such effects on reaction rates and selectivities.

3. Fixed-bed reactor calculations for isomerization of *n*-hexane

Consider a reactor filled with particles containing crystallites of MFI as catalyst for carrying out the isomerization of nC6 to produce a product containing mono-branched 3MP and di-branched 22DMB. For simplicity we consider only three hexane isomers instead of five and we take 3MP to

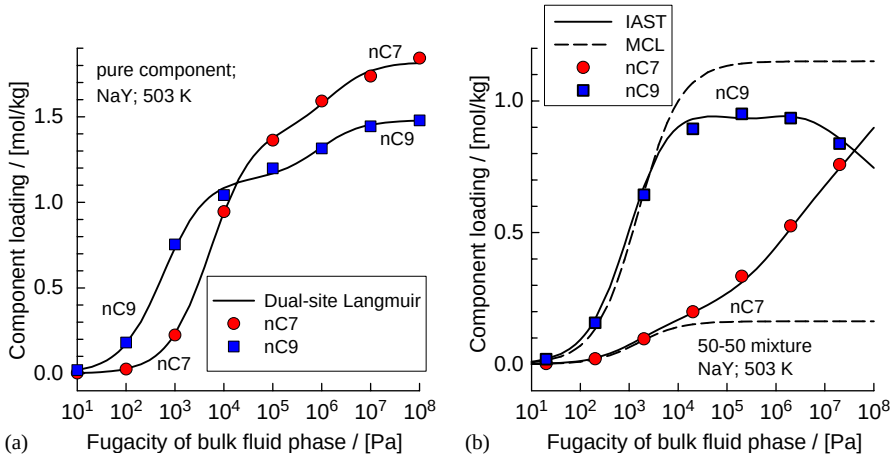

Fig. 5. (a) Pure component isotherms of nC7 and nC9 on NaY at 503 K determined by CBMC simulations (Calero et al., 2004). The continuous lines are the dual-Langmuir fits with the parameters specified in Table 2. (b) Component loadings in 50–50 mixture of nC7 and nC9 in NaY. The continuous solid lines are the calculation of the IAST using the DSL parameter fits as specified in Table 2. The dashed lines represent the calculations using the MCL model.

Table 2
DSL parameters for various components in NaY and AFI zeolites

Zeolite	Component	DSL parameters			
		Site A		Site B	
		$b_{i,A}$ [Pa^{-1}]	$q_{i,sat,A}$ [$molkg^{-1}$]	$b_{i,B}$ [Pa^{-1}]	$q_{i,sat,B}$ [$molkg^{-1}$]
NaY at 503 K	*n*C7	1.95×10^{-4}	1.42	6.84×10^{-7}	0.4
	*n*C9	1.801×10^{-3}	1.14	1.174×10^{-6}	0.34
AFI at 403 K	*n*C6	3.951×10^{-3}	0.54	1.045×10^{-4}	0.16
	3MP	5.376×10^{-3}	0.71	3.437×10^{-5}	0.15
	22DMB	3.052×10^{-3}	0.83	7.673×10^{-5}	0.14

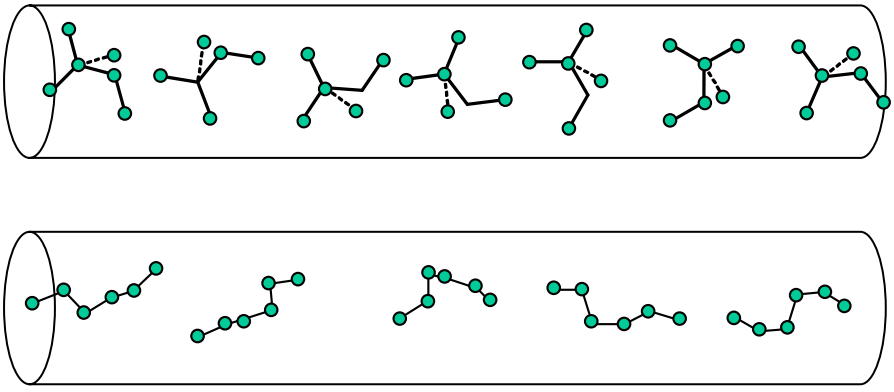

Fig. 6. Schematic of length entropy effect during sorption of *n*C6, 3MP and 22DMB in the cylindrical channels of AFI.

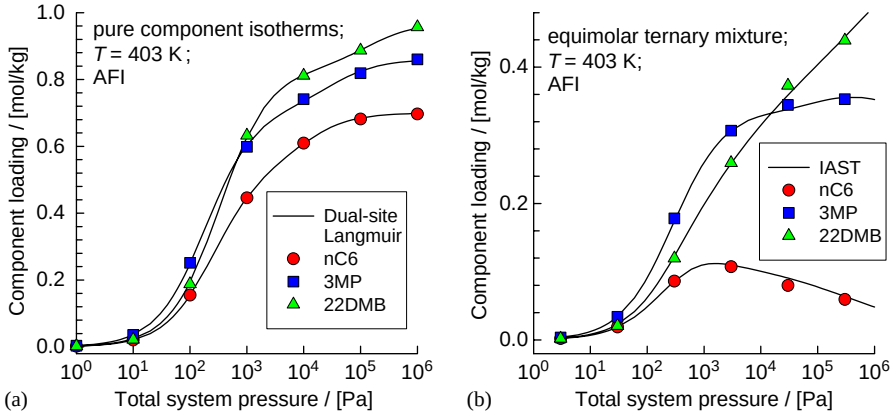

Fig. 7. (a) Pure component sorption isotherms for *n*C6, 3MP and 22DMB in AFI zeolite at 403 K. The symbols represent CBMC simulation data (Calero et al., 2001; Krishna et al., 2002b, Schenk et al., 2001b). The continuous solid lines are the DSL fits using the parameters as specified in Table 2. (b) Component loadings in equimolar ternary mixture of *n*C6, 3MP and 22DMB at 403 K. The symbols represent the CBMC simulations whereas the continuous solid lines represent calculations from IAST using the DSL parameters specified in Table 2.

represent single-branched isomers and 22DMB to be representative of di-branched isomers. From octane number considerations we wish to maximize the production of the di-branched isomer (Carr and Dandekar, 2001). We restrict our analysis to the simplified reaction scheme

$$n\text{C6} \rightleftarrows \text{3MP} \rightleftarrows \text{22DMB}, \quad (5)$$

where the LH reaction rate expressions for the two constituent reversible reactions are

$$r_1 = (k_{f1}p_1 - k_{b1}p_2)\theta_V; \quad r_2 = (k_{f2}p_2 - k_{b2}p_3)\theta_V, \quad (6)$$

where the subscripts f and b refer to the forward and reverse reactions, and the subscripts 1 and 2 refer to the first and second isomerization reaction steps in Eq. (5).

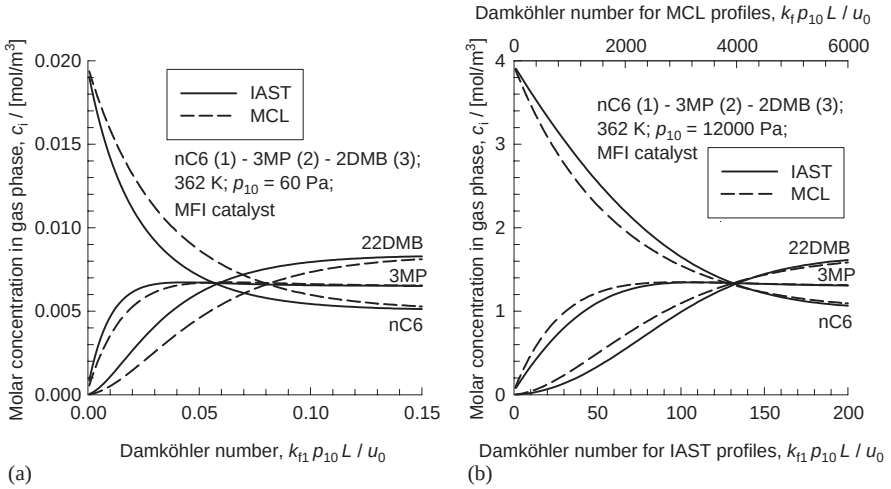

Fig. 8. Steady-state gas phase concentration profiles in a fixed bed hexane isomerization reactor packed with MFI catalyst and operating at 362 K. The inlet partial pressures of nC6 in the gaseous feed stream are (a) 60 Pa, and (b) 12,000 Pa. The total reactor pressure is maintained at 200 kPa, with the non-hydrocarbon portion being inert. The bed porosity $\varepsilon = 0.4$. The interstitial gas velocity at the inlet $u_0 = 0.071\,\mathrm{m\,s^{-1}}$. The MFI crystallites in the catalyst are small enough for intra-crystalline diffusional limitations to be considered absent. The continuous solid lines represent calculations using LH-IAST, with the DSL parameter inputs as specified in Table 1. Calculations of LH-MCL model are shown by the dashed lines. Note that in (b) the x-axis for the LH-MCL model is shown on the top.

From available information for the free energies of formation (Poling et al., 2001) we can estimate the values of the equilibrium constants k_{f1}/k_{b1} and k_{f2}/k_{b2}. On the basis of this information, along with data on reaction kinetics (van Donk et al., 2001) we take $k_{f1} = k_{f2} = 0.009\,\mathrm{Pa^{-1}s^{-1}}$ and $k_{b1} = k_{b2} = 0.007\,\mathrm{Pa^{-1}s^{-1}}$. We assume that the zeolite crystallites are small enough that intra-crystalline diffusion is not rate limiting. In practice a choice of crystallites smaller than about 1 μm, will ensure that diffusion is not important. The steady-state gas phase concentration profiles for a reactor with pure nC6 feed in the gas phase at a partial pressure $p_{10} = 60\,\mathrm{Pa}$ and temperature $T = 362\,\mathrm{K}$ is shown in Fig. 8a, as a function of the Damköhler number, $Da \equiv k_{f1} p_{10} L/u_0$ where L is the total length of the packed bed reactor.

The calculations using IAST for calculation of θ_V are shown with the continuous solid lines, whereas the MCL model for θ_V are shown with the dashed lines. Details of the numerical procedures used in the reactor calculations are available elsewhere (Krishna and Baur, 2003a). For the chosen feed partial pressure $p_{10} = 60\,\mathrm{Pa}$ both the LH-IAST and LH-MCL approaches yield approximately the same results for the concentration profiles in the gas phase, as is to be expected because entropy effects are practically absent in the Henry regime of adsorption. The situation changes dramatically when we consider the reactor concentration profiles for a pure nC6 feed at a partial pressure $p_{10} = 12,000\,\mathrm{Pa}$; the results are shown in Fig. 8b. The LH-IAST and LH-MCL calculations are shown by the solid and dashed lines, respectively, with the x-axes corresponding, respectively, to the bottom and top. We note that the LH-MCL model requires an order-of-magnitude higher value of Da to reach the equilibrium conversion in the reactor. This result could be anticipated in view of the θ_V values presented in Fig. 4. At equilibrium, the conversion of nC6 is 75% for both LH-IAST and LH-MCL approaches.

Since entropy effects cause significantly lower sorption loadings for the mono- and di-branched isomers at higher pressures (see Fig. 3), the branched products of the isomerization reaction are more easily desorbed into the gas phase than nC6. This fact is emphasized when we consider the transient approach to steady state for a fixed bed reactor with a nC6 feed partial pressure of 12,000 Pa, calculated using the more appropriate LH-IAST model. The transient development along the reactor length of the gas phase concentration profiles at times $t = 425$, 786 and 1100 s from time of feed introduction are shown in Figs. 9a–c. We note that the "front" on 22DMB travels ahead of that of 3MP, in view of the easier desorption from the catalyst. At the reactor exit, the "breakthrough" of the three isomers is shown in Fig. 9d. The initial product is almost pure 22DMB and only later do 3MP and nC6 appear in the product stream.

Fig. 10 shows the corresponding transient profiles calculated using the LH-MCL approach. The 22DMB and 3MP fronts travel at nearly the same velocity in view of the much lower sorption selectivity anticipated by the MCL model. In situ desorption of the desired product 22DMB can be expected to be a difficult proposition according to the MCL approach. On the other hand, in situ separation of the desired product 22DMB is clearly possible with the LH-IAST approach.

While a pulsed transient operation of a fixed bed reactor provides the proof of principle of in situ separation, for large scale continuous processing required by the petroleum industry we need to adopt the simulated moving bed reactor concept described below.

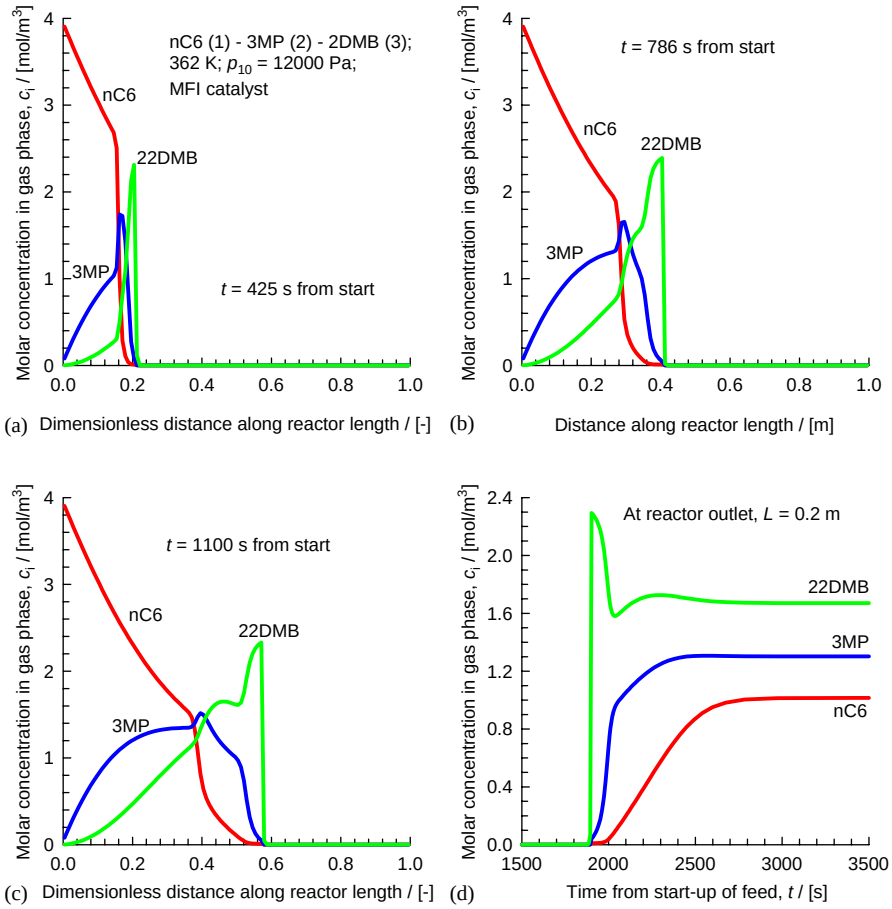

Fig. 9. Transient development of concentration profiles in a fixed bed hexane isomerization reactor packed with MFI catalyst and operating at 362 K, calculated using the LH-IAST approach. The reactor bed length $L = 0.2$ m, the bed porosity $\varepsilon = 0.4$, and the interstitial gas velocity at the inlet $u_0 = 0.071\,\mathrm{m\,s^{-1}}$. At time $t = 0$ the inlet partial pressure of nC6 in the gaseous feed stream is set to 12,000 Pa and maintained at this level. The total reactor pressure is maintained at 200 kPa, with the non-hydrocarbon portion being inert. The gas phase concentration profiles of nC6, 3MP and 22DMB along the reactor length at shown at various time intervals (a) $t = 425$ s, (b) $t = 786$ s, and (c) $t = 1100$ s. (d) The transient "breakthrough" of nC6, 3MP and 22DMB at the reactor outlet ($L = 0.2$ m) is shown as a function of time from introduction of feed to the reactor inlet.

4. Simulated moving bed reactor concept for hexane isomerization

The easier desorption of the product 22DMB, predicted by the more rigorous LH-IAST approach, gives us a clue as to how we can exploit entropy effect to achieve supra-equilibrium conversions and improved selectivity. The selectivity is defined as the ratio of 22DMB to 3MP in the product. The trick is to adopt the simulated moving bed (SMB) reactor concept, where the desired 22DMB product is "tapped" off at spatio-temporal positions where (when) it peaks. Since the 22DMB front moves ahead of the fronts of the other two species, the SMB concept offers the potential of not only improved nC6 conversion but also a higher 22DMB/3MP ratio in the product stream. We will demonstrate the feasibility of this concept by considering the SMB configuration containing 10 equally sized reactor segments as sketched in Fig. 11. The gaseous feed is introduced at position 0 and the product withdrawn at the exit of second reactor (position 2). The cycle time is taken to be 600 s. The inert gas stream serves to desorb the components from the catalyst phase. The desorption takes place predominantly in reactor segments 3–10. Further details are specified in the legend to Fig. 11. The chosen operating conditions for the SMB reactor (flow rates, switching frequencies, feed injection and product withdrawal strategies) were arrived at after a careful and detailed analysis. After each cycle is completed the feed and product withdrawal ports are switched by one position in the direction of gas flow. In this way we effectively achieve counter–current gas–catalyst contacting. The simulations were carried out till true quasi-steady-state conditions are achieved. The transient conversions and selectivities are shown in Figs. 12a,b. The nC6 conversion, obtained by time-averaging over the quasi-steady-state period is found to be 82%, which is significantly higher than the 75% conversion realized in a conventional fixed bed reactor mode. The time-averaged

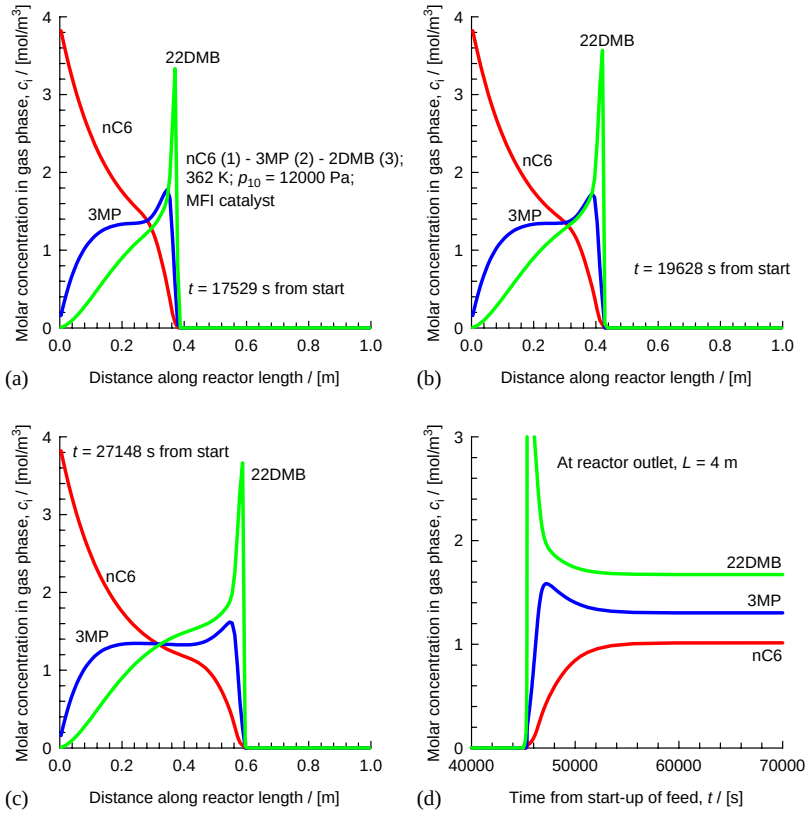

Fig. 10. Transient development of concentration profiles in a fixed bed hexane isomerization reactor packed with MFI catalyst and operating at 362 K, calculated using the LH-MCL approach. The reactor bed length $L = 4$ m, the bed porosity $\varepsilon = 0.4$, and the interstitial gas velocity at the inlet $u_0 = 0.071\,\mathrm{m\,s^{-1}}$. At time $t = 0$ the inlet partial pressure of nC6 in the gaseous feed stream is set to 12,000 Pa and maintained at this level. The total reactor pressure is maintained at 200 kPa, with the non-hydrocarbon portion being inert. The gas phase concentration profiles of nC6, 3MP and 22DMB along the reactor length at shown at various time intervals (a) $t = 17,529$ s, (b) $t = 19,628$ s, and (c) $t = 27,148$ s. (d) The transient "breakthrough" of nC6, 3MP and 22DMB at the reactor outlet ($L = 4$ m) is shown as a function of time from introduction of feed to the reactor inlet.

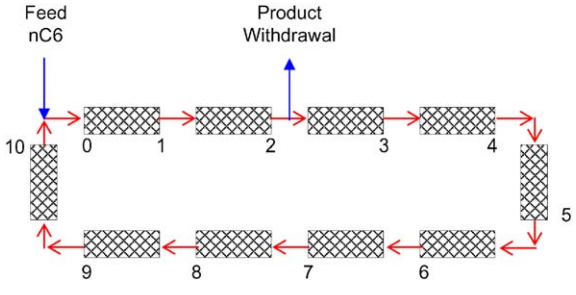

Fig. 11. Schematic of simulated moving bed (SMB) configuration. It consists of 10 fixed bed reactor elements of equal length, packed with zeolite catalyst particles bed porosity $\varepsilon = 0.4$. The MFI crystallites in the catalyst are small enough for intra-crystalline diffusional limitations to be considered absent. The inlet partial pressure of nC6 in the gaseous feed stream to the inlet of Reactor 1 (position 0) is 12,000 Pa. The total reactor pressure is maintained in all ten reactor segments at 200 kPa, with the non-hydrocarbon portion being inert. The products are withdrawn two reactor segments further down than the feed gas stream. The interstitial gas velocity u_0 is maintained constant $=0.071\,\mathrm{m\,s^{-1}}$ in all the reactor segments; this is done by replacing the withdrawn product with inerts at position 2. The total length of the packed section in all ten reactor segments, $L = 0.8$ m. After intervals of $t = 600$ s ($\tau = tu_0/L = 53.25$), the position of the feed and withdrawal points are shifted one step each.

22DMB/3MP ratio in the product under quasi-steady-state conditions is 1.42, compared to 1.28 for fixed bed reactor operation.

The gas phase concentration profiles along the SMB reactor segments are shown in Fig. 13 a just before the start of the feed injection, when quasi-steady state has been achieved. We note that the 22DMB concentration is higher than that of 3MP and nC6 in the desorption zones 3–10. Snapshots of the concentration profiles at times $t = 50$, 100 and 207 s after the start of feed injection are shown in Figs. 13b–d. We see that the 22DMB front moves ahead of that of 3MP and nC6 in the reactor segments 1 and 2. As a consequence during the product withdrawal process, we have an almost pure 22DMB product in the initial stages of the cycle. This explains high conversions, approaching 100%, near the start of the cycle (see Fig. 12a), which reduces to the equilibrium conversion value (75%) towards the end of the cycle. For the same reason the 22DMB/3MP ratio is highest towards the start of the cycle and reaches the equilibrium value of 1.28 near the end of the cycle.

There is some evidence in the patent literature concerning the benefits of SMB reactor operation for zeolite catalysed

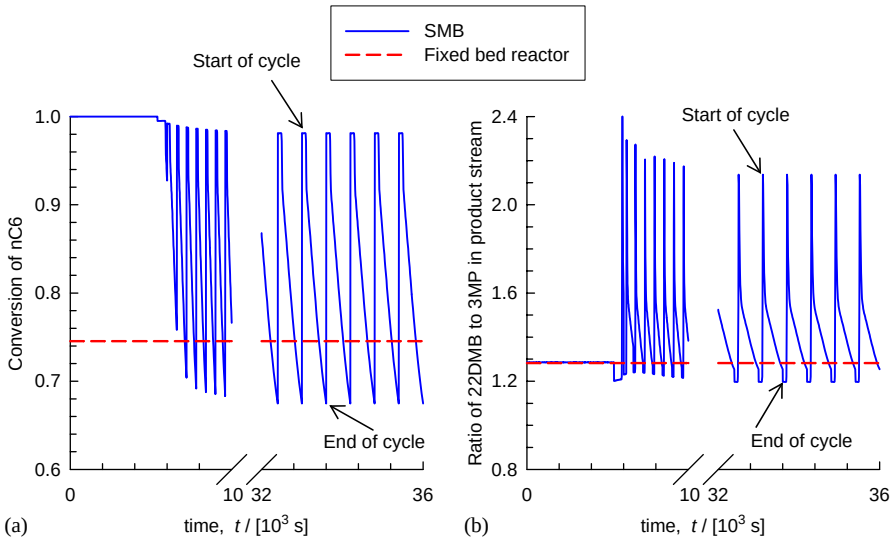

Fig. 12. Transient analysis of the gaseous products withdrawn in the SMB reactor. (a) The conversion of *n*C6 as a function of time. (b) The ratio of 22DMB to 3MP in the gaseous product stream as a function of time.

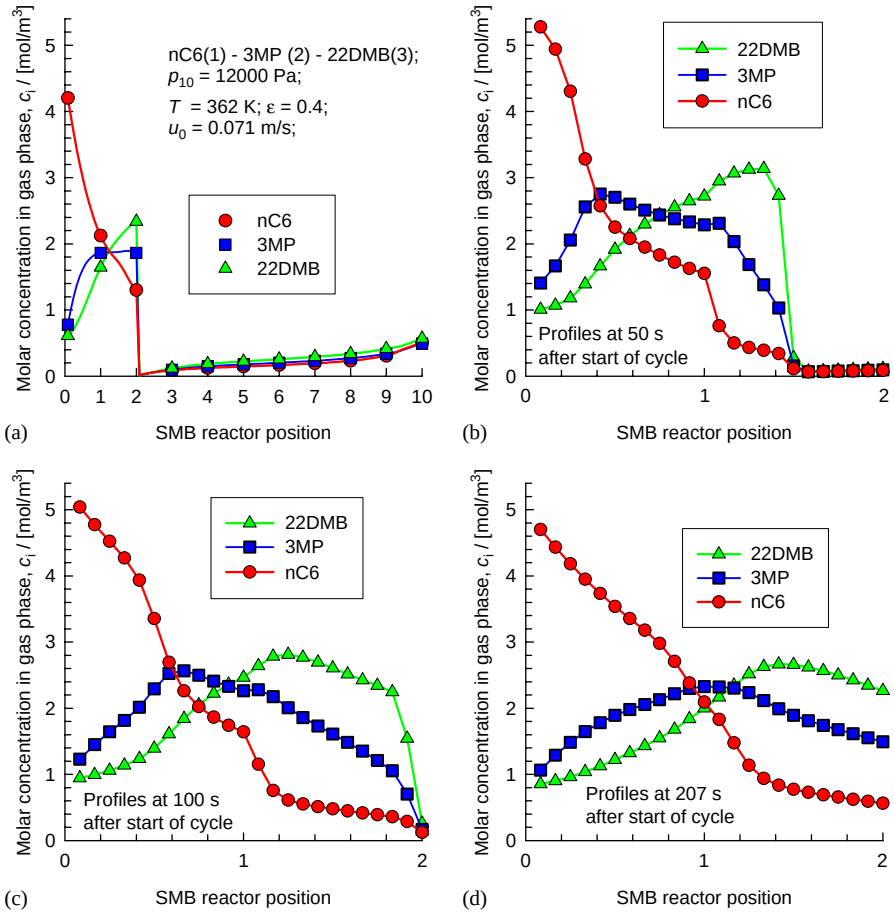

Fig. 13. Concentration profiles in the SMB reactor under quasi-steady-state conditions. (a) The gas phase concentrations of *n*C6, 3MP, and 22DMB along all the reactor segments $(1, 2, 3 \ldots 10)$ at the start of a new cycle (of 600 s duration). (b) Concentration profiles in the reacting segments 1 and 2 at $t = 50$ s from start of the cycle. (c) Concentration profiles in the reacting segments 1 and 2 at $t = 100$ s from start of the cycle. (d) Concentration profiles in the reacting segments 1 and 2 at $t = 207$ s from start of the cycle.

hexane isomerization with respect to improved octane of the product (Dandekar et al., 1998, 2000). These patents do not, however, specify which specific zeolite is suitable for the task. The analysis presented in the foregoing shows that MFI zeolite is suitable for this task because it has the correct sorption hierarchy 22DMB > 3MP > *n*C6. In this context it must be stressed that MOR zeolite (used in conventional fixed bed reactor technologies currently in commercial use) is unsuitable because the sorption hierarchy is reverse of the desired on (Krishna et al., 2002b). With MOR catalyst the leading front will be the reactant *n*C6, which is clearly undesirable from the viewpoint of in situ separation. Another important consideration in SMB reactor operation is that we must operate under conditions such that the loadings within the zeolite catalyst are maintained at a level higher than 4 molecules per unit cell, to ensure that entropy effects dominate the sorption strengths. To properly describe and model entropy effects in zeolite catalysis, we must abandon the conventionally used LH-MCL formulation (3) and adopt the more rigorous LH-IAST model.

5. Conclusions

In this paper we have stressed the limitations of the commonly used kinetic expression (3), which combines the original LH reaction rate concept (1) with the MCL expression (2) for estimation of the fractional loadings and vacancy θ_V. The MCL approach is applicable only when the saturation capacities of all the species in the mixture are identical. The MCL approach is also applicable for low loadings in the Henry regime. For the general case, where the saturation capacities of the individual species are significantly different and the operation is at high loadings, entropy effects have a significant influence on the sorption hierarchy and on the occupancies. For sorption of hexane isomers in MFI zeolite, for example, entropy effects arise because of the differences in the efficiencies with which the linear and branched isomers pack within the zeolite topology. With increased degree of branching the packing efficiency becomes poorer at high loadings and therefore mono- and di-branched isomers are virtually excluded from the zeolite matrix near saturation loadings. In order to account for entropy effects on sorption, we need to adopt the more rigorous IAST for calculation of component loadings and occupancies.

Using a specific example of the isomerization of hexane *n*C6⇄3MP⇄22MP we have demonstrated the significant differences in the reaction rates anticipated by the LH-MCL and LH-IAST approaches. More significantly, we have shown that recognition of entropy effects allows us to exploit entropy effects to improve the conversion and selectivity by adopting the SMB reactor concept. Such exploitation is impossible with the conventionally used LH-MCl approach.

Notation

b_i	parameter in the pure component Langmuir adsorption isotherm, Pa^{-1}
c_i	molar concentration of species i, mol m^{-3}
Da	Damköhler number, $Da \equiv k_{f1} p_{10} L/u_0$, dimensionless
f_i	fugacity of species i; $f_i = p_i$ for ideal gases, Pa
k_f	forward reaction rate constant, $Pa^{-1}\,s^{-1}$
k_b	backward reaction rate constant, $Pa^{-1}\,s^{-1}$
L	Length of packed bed reactor, m
n	index in θ_V^n reflecting n-molecular reaction, dimensionless
p_i	partial pressure of species i, Pa
q_i	molar loading of component i, mol kg^{-1}
q_{sat}	saturation loading, mol kg^{-1}
r	reaction rate, s^{-1}
t	time, s
T	absolute temperature, K
u_0	interstitial fluid velocity in packed bed, m s^{-1}

Greek letters

ε	porosity of packed bed of zeolite catalyst, dimensionless
θ_i	fractional occupancy of component i, dimensionless
Θ_i	molecular loading of species i, molecules per unit cell
$\Theta_{i,sat}$	saturation loading of species i, molecules per unit cell
τ	dimensionless residence time, dimensionless

Subscripts

1	referring tospecies 1
2	referring to species 2
A	referring to site A
B	referring to site B
i	referring to species i
sat	referring to saturation conditions
V	referring to vacant sites in zeolite

Acknowledgements

RB and RK acknowledge a grant *Programmasubsidie* from the Netherlands Foundation for Fundamental Research (CW-NWO) for development of novel concepts in reactive separations. Dr. S. Calero performed the CBMC simulation results presented in Figs. 1, 3, 5, and 7.

References

Aris, R., 1975. The Mathematical Theory of Diffusion and Reaction in Permeable Catalysts, Clarendon Press, Oxford.

Calero, S., Smit, B., Krishna, R., 2001. Configurational entropy effects during sorption of hexane isomers in silicalite. Journal of Catalysis 202, 395–401.

Calero, S., Dubbeldam, D., Krishna, R., Smit, B., Vlugt, T.J.H., Denayer, J.F.M., Martens, J.A., Maesen, T.L.M., 2004. Understanding the role of sodium during adsorption. A force field for alkanes in sodium exchanged faujasites. Journal of the American Chemical Society 126, 11376–11385.

Carr, R.W., Dandekar, H.W., 2001. Adsorption with reaction. In: Kulprathipanja, S. (Ed.), Reactive Separation Processes. Taylor & Francis, New York, USA.

Corma, A., 2003. State of the art and future challenges of zeolites as catalysts. Journal of Catalysis 216, 298–312.

Dandekar, H.W., Funk, G.A., Gillespie, R.D., Zinnen, H.A., McGonegal, C.P., Kojima, M., Hobbs, S.H., 1998. Process for alkane isomerization using reactive chromatography. US 5763730, UOP Inc., USA.

Dandekar, H.W., Funk, G.A., Zinnen, H.A., 2000. Process for separating and recovering multimethyl-branched alkanes. US 6069289, UOP Inc., USA

Degnan, J., Thomas, F., 2003. The implications of the fundamentals of shape selectivity for the development of catalysts for the petroleum and petrochemical industries. Journal of Catalysis 216, 32–46.

Denayer, J.F.M., Ocakoglu, R.A., Huybrechts, W., Dejonckheere, B., Jacobs, P., Calero, S., Krishna, R., Smit, B., Baron, G.V., Martens, J.A., 2003. High pressure liquid phase hydroconversion of heptane/nonane mixture on Pt/H-Y zeolite catalyst. Journal of Catalysis 220, 66–73.

van Donk, S., Broersma, A., Gijzeman, O.L.J., van Bokhoven, J.A., Bitter, J.H., de Jong, K.P., 2001. Combined diffusion, adsorption, and reaction studies of *n*-hexane hydroisomerization over Pt/H-mordenite in an oscillating microbalance. Journal of Catalysis 204, 272–280.

Dubbeldam, D., Calero, S., Vlugt, T.J.H., Krsihna, R., Maesen, T.L.M., Smit, B., 2004. United atom forcefield for alkanes in nanoporous materials. Journal of Physical Chemistry B 108, 12301–12313.

Kapteijn, F., Moulijn, J.A., Krishna, R., 2000. The generalized Maxwell–Stefan model for diffusion in zeolites: sorbate molecules with different saturation loadings. Chemical Engineering Science 55, 2923–2930.

Krishna, R., Baur, R., 2003a. Diffusion, adsorption and reaction in zeolites: modelling and numerical issues. http://ct-cr4.chem.uva.nl/zeolite/, 10 November 2003.

Krishna, R., Baur, R., 2003b. Modelling issues in zeolite based separation processes. Separation and Purification Technology 33, 213–254.

Krishna, R., Calero, S., Smit, B., 2002a. Investigation of entropy effects during sorption of mixtures of alkanes in MFI zeolite. Chemical Engineering Journal 88, 81–94.

Krishna, R., Smit, B., Calero, S., 2002b. Entropy effects during sorption of alkanes in zeolites. Chemical Society Reviews 31, 185–194.

Marcilly, C., 2003. Present status and future trends in catalysis for refining and petrochemicals. Journal of Catalysis 216, 47–62.

Myers, A.L., Prausnitz, J.M., 1965. Thermodynamics of mixed gas adsorption. American Institute of Chemical Engineers Journal 11, 121–130.

Poling, B.E., Prausnitz, J.M., O'Connell, J.P., 2001. The Properties of Gases and Liquids, fifth ed. McGraw-Hill, New York.

Rao, M.B., Sircar, S., 1999. Thermodynamic consistency for binary gas adsorption equilibria. Langmuir 15, 7258–7267.

Schenk, M., Smit, B., Vlugt, T.J.H., Maesen, T.L.M., 2001a. Shape selectivity in hydrocarbon conversion. Angewandte Chemie-International Edition 40, 736–739.

Schenk, M., Vidal, S.L., Vlugt, T.J.H., Smit, B., Krishna, R., 2001b. Separation of alkane isomers by exploiting entropy effects during adsorption on silicalite-1. A configurational-bias Monte Carlo simulation study. Langmuir 17, 1558–1570.

Sircar, S., 1995. Influence of adsorbate size and adsorbent heterogeneity on IAST. American Institute of Chemical Engineers Journal 41, 1135–1145.

Sircar, S., Rao, M.B., 1999. Effect of adsorbate size on adsorption of gas mixtures on homogeneous adsorbents. American Institute of Chemical Engineers Journal 45, 2657–2661.

Vlugt, T.J.H., Krishna, R., Smit, B., 1999. Molecular simulations of adsorption isotherms for linear and branched alkanes and their mixtures in silicalite. Journal of Physical Chemistry B 103, 1102–1118.